

# Nonlinear field-dependence and $f$ -wave interactions in superfluid $^3\text{He}$

C.A. Collett, J. Pollanen, J.I.A. Li, W.J. Gannon, and W.P. Halperin

*Department of Physics and Astronomy, Northwestern University, Evanston, IL 60208, USA.*

(Dated: August 14, 2012)

We present results of transverse acoustics studies in superfluid  $^3\text{He}$ -B at fields up to 0.11 T. Using acoustic cavity interferometry, we observe the acoustic Faraday effect for a transverse sound wave propagating along the magnetic field, and we measure Faraday rotations of the polarization as large as  $1710^\circ$ . We use these results to determine the Zeeman splitting of the Imaginary Squashing mode (ISQ) frequency,  $\Omega$ , an order parameter collective mode with total angular momentum  $J = 2$ . We also report nonlinear field effects to the Faraday rotation, and find that theoretical predictions for the field dependence of the transverse acoustic dispersion relation, appropriate for frequencies near  $\Omega$ , cannot account for our data at frequencies substantially above the mode frequency. We determine the Landé  $g$ -factor describing the Zeeman effect for the mode, and the superfluid  $f$ -wave interaction strength,  $x_3^{-1}$ , after extrapolation of the acoustic frequency to the mode frequency, and we show that the pairing interaction in the  $f$ -wave channel is attractive at a pressure of  $P = 6$  bar, in good agreement with previous work. We have reanalyzed earlier results for the Faraday rotation with this extrapolation procedure, and we find that the  $f$ -wave interaction is attractive at all pressures.

PACS numbers: 43.35.Lq, 67.30.H-, 74.20.Rp, 74.25.Ld

## I. INTRODUCTION

Collisionless transverse sound was first predicted to exist in normal  $^3\text{He}$  by Landau<sup>1</sup>, but has not yet been experimentally detected. Moores and Sauls<sup>2</sup> showed that transverse mass currents couple to a collective mode of the order parameter, the Imaginary Squashing mode (ISQ), which has total angular momentum  $J = 2$ , leading to a propagating transverse sound mode in  $^3\text{He}$ -B. This coupling, and the presence of transverse sound in superfluid  $^3\text{He}$ , was demonstrated in 1999 by Lee *et al.*<sup>3</sup> Subsequently, transverse sound has been exploited as a probe of the excitation spectrum of  $^3\text{He}$ -B. Recent measurements at frequencies near the pair breaking threshold led to the discovery of a  $J = 4^-$  order parameter collective mode.<sup>4</sup>

Transverse sound provides a highly sensitive spectroscopy for the ISQ and its dependence on magnetic field. The frequency of this collective mode in zero field has been shown to be<sup>5,6</sup>  $\Omega_0 \sim \sqrt{12/5}\Delta$ , where  $\Delta$  is the weak-coupling-plus gap.<sup>7</sup> In a magnetic field  $\Omega$  splits into five Zeeman sub-states of which only two couple to transverse sound.<sup>2</sup> It is this splitting that is responsible for an Acoustic Faraday Effect (AFE), for which the observation by Lee *et al.*<sup>3</sup> is proof that transverse sound is a robust acoustic mode in superfluid  $^3\text{He}$ . The theory of Moores and Sauls<sup>2</sup> shows that right circularly-polarized (RCP) and left circularly-polarized (LCP) sound couple to opposing Zeeman states  $m_J = \pm 1$ , causing acoustic circular birefringence of a propagating linearly polarized transverse sound wave. When the field strength increases, the difference between the velocities of RCP and LCP increase proportionately, resulting in a rotation of a linearly polarized acoustic wave.

The coupling between transverse sound and the ISQ is

described by the following dispersion relation,

$$\frac{\omega^2}{q^2 v_F^2} = \Lambda_0 + \Lambda_{2-} \frac{\omega^2}{\omega^2 - \Omega^2(T, P, H) - \frac{2}{5} q^2 v_F^2}, \quad (1)$$

where  $\omega$  is the sound frequency,  $q$  the wavevector, and  $v_F$  the Fermi velocity. The quasiparticle restoring force is  $\Lambda_0 = \frac{F_1^s}{15}(1-\lambda)(1+\frac{F_2^s}{5})/(1+\lambda\frac{F_2^s}{5})$ , and  $\Lambda_{2-} = \frac{2F_1^s}{75}\lambda(1+\frac{F_2^s}{5})^2/(1+\lambda\frac{F_2^s}{5})$  is the superfluid coupling strength, where  $F_1^s, F_2^s$  are Landau parameters, and  $\lambda$  is the Tsuneto function.<sup>8</sup> Up to linear order in magnetic field,  $H$ , the splitting of the ISQ is expected to modify the denomina-

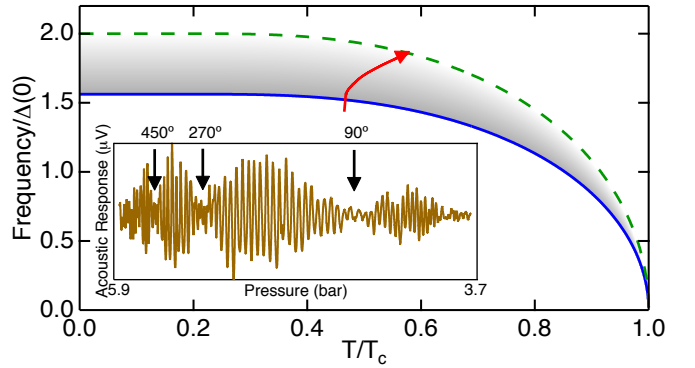


FIG. 1. Frequencies of the ISQ (blue line) and pair-breaking edge (green dashed line) as a function of reduced temperature. The grey shaded area is the region supporting transverse sound. The red arrow indicates the path of the sound frequency, normalized to the pressure dependent gap, during a typical decreasing pressure sweep. Inset: A representative acoustic response versus pressure measured between the ISQ and pair-breaking, taken on a path similar to that indicated by the red arrow, at  $H = 0.04$  T, with the visible minima, indicated by black arrows, corresponding to AFE rotations of  $90^\circ$ ,  $270^\circ$ , and  $450^\circ$ .

tor on the right-hand side of Eq. 1 to be

$$\omega^2 - \Omega_0^2 - \frac{2}{5}q^2v_F^2 - 2m_Jg\gamma_{\text{eff}}H\omega. \quad (2)$$

Here  $\gamma_{\text{eff}}$  is the effective gyromagnetic ratio of  $^3\text{He}$  and  $g$  is the Landé  $g$ -factor of the ISQ.

In the work we report here we have extended our study of transverse sound<sup>6</sup> in two ways: to large magnetic fields entering a regime where the ISQ is nonlinear in  $H$ , and to high frequencies well away from the mode crossing between the acoustic frequency and that of the ISQ collective mode. These reveal behavior not accounted for by Eq. 2. We are able to accurately extrapolate to the linear field regime and close to the mode crossing condition where we can compare with the theory, which is defined near the mode. Based on this comparison, we provide accurate results for the  $g$ -factor, which is sensitive to  $f$ -wave pairing interactions. The dominant pairing in superfluid  $^3\text{He}$  is  $p$ -wave; nonetheless, higher order interactions are relevant to order parameter dynamics. Sauls and Serene predicted<sup>9</sup> that  $g$  would depend on  $f$ -wave contributions, those having relative angular momentum  $l = 3$ , and we use  $g$  to quantify those contributions.

In an early study of the field dependence of the ISQ, Movshovich *et al.*<sup>10</sup> made measurements up to 0.46 T with longitudinal sound, which is strongly coupled to the ISQ. This coupling causes large extinction regions around the mode frequency, making it impossible to differentiate different angular momentum substates at low fields. Thus, high fields were required to distinguish the signatures of the substates, with only a few data points for fields below 0.1 T.

In contrast to longitudinal sound, the transverse mode is weakly coupled to the ISQ and consequently has much higher spectral resolution. Lee *et al.*<sup>3</sup> fixed the sound frequency and swept the temperature in fields up to 0.015 T. Sweeping temperature or pressure changes the wavelength of the sound giving rise to an oscillatory acoustic cavity response according to  $\omega d/\pi c_t$ , where  $c_t$  is the transverse sound velocity and  $d$  is the size of the acoustic cavity, typically 30  $\mu\text{m}$  in our experiments. For a magnetic field along the sound propagation axis the sound polarization rotates with respect to the initial polarization axis of the sound producing a modulation of the oscillatory response with a node at magnetic fields that correspond to odd integer multiples of a  $90^\circ$  rotation of the polarization within the cavity (see the trace in the inset to Fig. 1). The magnitude of the rotation is proportional to the magnetic field in the low field limit owing to the linear Zeeman splitting of the ISQ. This acoustic Faraday effect was used by Lee *et al.* to calculate the Landé  $g$ -factor of the order parameter collective mode. Davis *et al.*<sup>6</sup> extended these AFE experiments to a field  $H \approx 0.04$  T and also reported data over a wide range of pressures in order to determine the pressure dependence of the  $g$ -factor. The latter measurements were performed by temperature sweep with sound frequencies well above the mode frequency,  $\omega > \Omega_0$ .

In addition to the AFE, an applied magnetic field induces acoustic circular dichroism. The absorption coefficients of RCP and LCP depend on  $m_J$ , and in a field they split, causing one polarization to be attenuated more than the other. This has the effect of both flattening and shifting the Faraday rotation envelope. These effects are not significant in fields in the kG range, and so do not play a role for the field strengths used in these experiments.

Davis *et al.*<sup>6</sup> observed linear field effects at low field, while Movshovich *et al.*<sup>10</sup> saw quadratic behavior at high field. Thus the intermediate field region, where nonlinear field effects become significant, has remained relatively unexplored. In addition, Davis *et al.*<sup>6</sup> found an unexpected temperature dependence to  $g$  that they were unable to identify, and so they focused only on measurements extrapolated to  $T = 0$ . In the present work we explore both the intermediate field region and regions of frequency well above the ISQ-mode frequency. This allows us to make a precise identification of the low-field, linear Zeeman splitting and the corresponding  $f$ -wave pairing interactions in superfluid  $^3\text{He}$ .

## II. EXPERIMENTS

Our experimental setup is functionally the same as that described previously.<sup>6</sup> To probe the Faraday rotation, we cool liquid  $^3\text{He}$  to  $\sim 600$   $\mu\text{K}$  in an acoustic cavity formed by a transducer and a quartz reflecting plate and then slowly decrease the pressure in the cell from  $\sim 6$  to 3 bar. This pressure change continuously alters the frequencies of pair-breaking and the ISQ relative to a fixed transducer frequency of 88 MHz. Accordingly, the sound frequency passes through the ISQ and approaches pair-breaking along a trajectory similar to the red curve in Fig. 1. As the difference between  $\omega$  and  $\Omega$  increases with decreasing pressure, both the transverse sound velocity,  $c_t = \omega/q$ , and the wavelength decrease, changing the standing wave condition in the acoustic cavity. This produces the high-frequency oscillations shown in the inset of Fig. 1. As previously discussed, application of a magnetic field along the direction of sound propagation rotates the sound polarization, and this is seen as a modulation of the acoustic cavity oscillations. Both effects are described by

$$V_Z \propto \cos \theta \sin \left( \frac{2d\omega}{c_t} \right), \quad (3)$$

where  $V_Z$  is the detected transducer voltage,  $\theta$  is the angle of the sound polarization relative to the direction in which sound was generated, and  $d = 31.6 \pm 0.1$   $\mu\text{m}$  is the cavity spacing.<sup>6</sup>

In order to convert an acoustic trace into a form that can be related to the dispersion relation, Eq. 1, we first apply Eq. 3 to extract  $\theta$  and  $c_t$ . From the sinusoidal dependence of  $V_Z$  on  $\theta$ , we identify minima in the envelope as the polarization rotation angles  $\theta =$

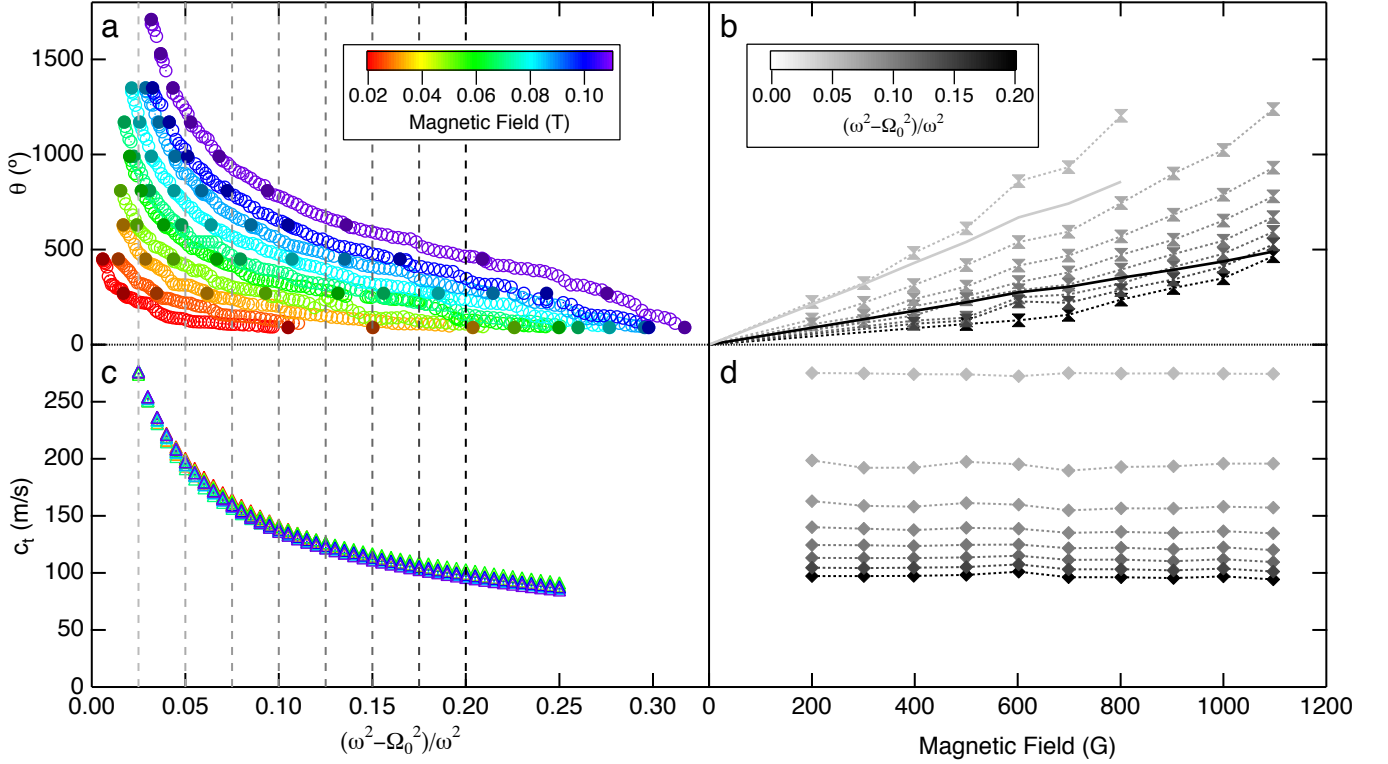


FIG. 2. (a) Data for AFE rotation angle,  $\theta$ , at all experimental fields, as a function of shift. The solid circles correspond to minima in the acoustic trace. The dashed lines indicate the shift values for which data is presented in (b). (b)  $\theta$  data at selected values of  $(\omega^2 - \Omega_0^2)/\omega^2$  as a function of field, demonstrating nonlinear behavior and a decrease in  $\theta$  as a function of distance from the ISQ. The dotted lines directly join the data points, and are presented solely as guides to the eye. The solid lines indicate the  $\theta$  values expected from the dispersion for linear splitting at constant  $g = 0.049$  at the lowest (light grey) and highest (black) shifts presented, exhibiting less than two thirds the decrease shown in the data. (c) Sound velocity,  $c_t$ , data at all experimental fields, as a function of shift; the data points overlap at each shift value. The dashed lines indicate the shift values for which data is presented in (d). (d)  $c_t$  data at the same shift values as in (b), demonstrating the lack of observed field dependence of  $c_t$ .

$n \times 90^\circ$ ;  $n = 1, 3, 5, \dots$ , and calculate intermediate angles from the modulation. Also from  $V_Z$ , we measure the period of the high-frequency oscillations,

$$1 \text{ Period} = 2d \frac{\omega}{2\pi} \left| \frac{1}{c_{tf}} - \frac{1}{c_{ti}} \right|. \quad (4)$$

that results from the change of the sound velocity. We use Eq. 1 to calculate an initial value of the velocity where the theoretical formula is accurate near resonance,  $\omega \approx \Omega$ , in order to determine  $c_t$  from Eq. 4.

### III. RESULTS AND DISCUSSION

#### A. Data

Our  $\theta$  and  $c_t$  data are displayed in Fig. 2. The abscissa in Fig. 2(a), (c), and several of the following figures, is the normalized difference in the square of the frequencies,  $(\omega^2 - \Omega_0^2)/\omega^2$ . In the following we will refer to this as the relative frequency shift, or just the shift. We use this scaling in preference to more direct variables such as pressure

or temperature because it is a more explicit measure of changes in the dispersion that take place as the pressure or temperature change. During a typical pressure sweep the temperature also increases slightly and both of these dependencies are reflected in  $\Omega(P, T)$ .<sup>5</sup> The (b) and (d) panels in Fig. 2 are the values of  $\theta$  and  $c_t$  at specific shifts versus magnetic field, taken as vertical cuts indicated by the dashed lines in panels (a) and (c). It is immediately clear that the transverse sound velocity is relatively insensitive to the magnetic field while the Faraday rotation angle,  $\theta$  in Fig. 2(b), is predominantly linear in field at low fields, but becomes nonlinear at higher fields. Additionally, there is a substantial decrease in the linear field term with increasing  $(\omega^2 - \Omega_0^2)/\omega^2$  which we find to be inconsistent with the theory of the dispersion<sup>8</sup> expressed by Eq. 2.

#### B. Dispersion

The dispersion, in the form attained by combining Eqs. 1 and 2, can be solved to produce the Faraday rotation

angle, given the temperature, pressure, and  $g$ , neglecting nonlinear effects for now. During a decreasing pressure sweep there is a slight rise in the temperature, causing an increase in  $(\omega^2 - \Omega_0^2)/\omega^2$ . If  $g$  were independent of shift the  $\theta$  values calculated from the dispersion would show a decrease in the linear field dependence with increasing shift, as shown by the relative slopes of the solid lines in Fig. 2(b), but the magnitude of that decrease is less than two thirds that of our data. However, we should also allow for the fact that the theory of Sauls and Serene<sup>9</sup> predicts that  $g$  depends weakly on both  $T$  and  $P$ . For the range of our data,  $P \sim 6 \rightarrow 4$  bar and  $T/T_c \sim 0.47 \rightarrow 0.64$ , the maximal expected change is  $\delta g \sim +0.008$ , which widens the discrepancy between data and theory even further by  $\sim 13\%$ . Therefore, the  $(\omega^2 - \Omega_0^2)/\omega^2$  dependence of the Faraday rotation angle we measure is incompatible with the theory of the transverse sound dispersion, Eq. 2, which was formulated for the near vicinity of the collective mode.<sup>8</sup>

The experiments by Movshovich *et al.* were performed at crossing,  $\omega = \Omega$ , and so they measured the field dependence directly.<sup>10</sup> In contrast, the transverse sound experiments in our work, as well as those of Davis *et al.*,<sup>6</sup> explore the full region of frequency between  $\Omega$  and  $2\Delta$ , where the dispersion relation, Eq. 2, may not be applicable.

To provide a framework for analysis we take a phenomenological approach making an assumption that the denominator on the right-hand side of the dispersion can be expanded in orders of field including terms up to  $H^3$ . We take Eq. 2 to be of the form

$$\begin{aligned} \omega^2 - \Omega_0^2 - \frac{2}{5}q^2v_F^2 - m_J A \gamma_{\text{eff}} H \\ - m_J^2 B \gamma_{\text{eff}}^2 H^2 - m_J^3 C \gamma_{\text{eff}}^3 H^3, \end{aligned} \quad (5)$$

where the terms containing  $A$ ,  $B$ , and  $C$  describe linear, quadratic, and cubic magnetic field dependences, respectively. As transverse sound couples only to the  $m_J = \pm 1$  substates, the linear and cubic terms switch signs for different substates, while the quadratic term is always negative since  $m_J^2 = 1$ . Within this framework, our choices for  $m_J$  are consistent with the theoretical field dependence for  $\Omega(H)$ .<sup>11,12</sup>

### C. Analysis

We can relate both Faraday rotation angle and sound velocity data to the modified dispersion of the ISQ found by inserting Eq. 5 into Eq. 1. It is helpful to use the following definitions:<sup>8,13</sup>

$$\theta = 2d\delta q, \quad (6)$$

$$c_t = 2\omega/(q_+ + q_-), \quad (7)$$

where  $\delta q = |q_+ - q_-|/2$ , and  $q_{\pm}$  is obtained by solving Eq. 1 for  $q$ , setting  $m_J = \pm 1$ . Because  $c_t$  is inversely proportional to the average of  $q_{\pm}$ , its dependence on linear

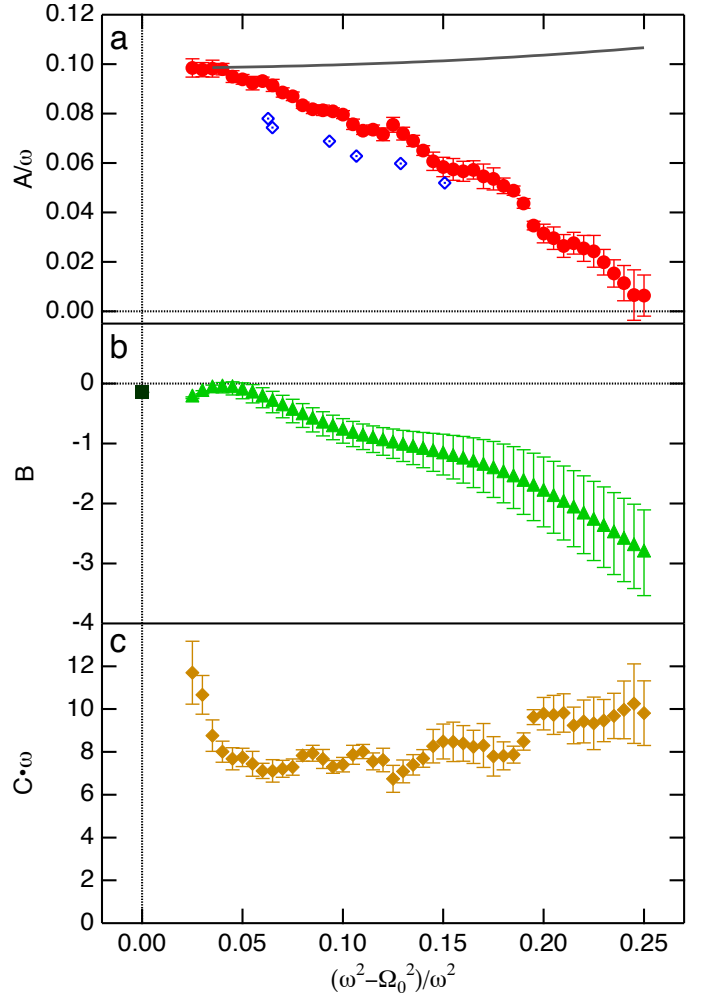


FIG. 3. Field dependence parameters  $A$ ,  $B$ , and  $C$  for Eq. 5, normalized to appropriate orders of  $\omega$  to make them dimensionless, plotted against shift. (a)  $A/\omega$  quantifies the linear field dependence, with the results from this work given by red circles, and for data from Davis *et al.*<sup>6</sup> at  $P = 4.7$  bar shown as open blue diamonds, which we have reanalyzed as discussed later in the text. At low shift the dominant contribution to  $A/\omega$  is from the Zeeman splitting of the ISQ and for which the theory<sup>8</sup> should be applicable. This splitting is predicted<sup>9</sup> to change slightly with  $T$  and  $P$  for a typical pressure sweep as shown by the grey line. There are other important contributions to  $A$  for frequencies well away from the ISQ mode, not described by the theory. (b)  $B$  identifies an upper bound on the quadratic field dependences, green triangles. The result from Movshovich *et al.*<sup>10</sup> is shown as a black square at  $\omega = \Omega_0$ , consistent with our results. (c) The cubic field parameter,  $C \cdot \omega$ , is shown as solid orange diamonds, not as reliably determined near the mode at low shift where there appears to be an upturn.

and cubic field terms cancels. Thus, the sound velocity depends at most on the quadratic field term. Conversely,  $\theta$  depends most strongly on the linear and cubic terms since the quadratic term is suppressed in the difference between  $q_+$  and  $q_-$ .

Examination of the data in Fig. 2(c) shows that  $c_t$  varies little, if at all, with field. To make this more explicit we separate the  $c_t$  data into bins of width  $(\omega^2 - \Omega_0^2)/\omega^2 = 0.005$ , and plot each bin as a function of field in Fig. 2(d) to display the (weak) dependence. We can at best establish an upper bound for the quadratic dependence of  $c_t$  on field found by fitting the  $c_t$  data with  $B$  as the only free parameter and setting  $A = C = 0$ , shown by green triangles in Fig. 3(b).

Nonlinear magnetic field effects play a significant role in  $\theta$ , as seen in Fig. 2(b). If we use the values for  $B$  established as a bound on the quadratic terms, we find that the effect of a quadratic field dependence on  $\theta$  is negligible. In order to describe the observed nonlinearity we must include the cubic field term in Eq. 5 containing the coefficient  $C$  in our  $\theta$  fits. With the addition of a cubic field term our model describes the data well. The best fit values for  $A$ ,  $B$ , and  $C$  are shown in Fig. 3, normalized to appropriate orders of  $\omega$  to render them dimensionless. The fitting is performed self-consistently with care to ensure that the initial sound velocity, constrained by the theory, is correctly represented. The grey line in Fig. 3(a) is an extrapolation of the theory<sup>8,9</sup> to frequencies well above the mode frequency, outside of its range of validity, which illustrates the discrepancy between our data and the theory. The relative importance of linear, quadratic and cubic terms in Eq. 5, *i.e.*  $A$ ,  $B$ , and  $C$ , on calculated values of  $\theta$  and  $c_t$  is displayed in Fig. 4 and described in the caption.

#### IV. NONLINEAR SPLITTING

We can compare our results for a bound on  $B$  with that of Movshovich *et al.*<sup>10</sup> Their value for  $B$  is presented as the black square in Fig. 3(b). This was taken from the nonlinear effects seen in the  $m_J = 0$  substate, and analyzed assuming a field dependence of the form

$$\Omega(H) = \Omega_0 + \alpha m_J H + \beta m_J^2 H^2 - \Gamma H^2, \quad (8)$$

leaving only the  $\Gamma$  term to affect the field dependence of the  $m_J = 0$  state. Assuming that same form, our result combines the quadratic field terms,  $B = \beta - \Gamma$ , and so we can only say that their result appears to lie within the bound we have set from our measurement of the field dependence of the velocity of transverse sound. Their analysis did not include the possibility of a cubic field dependence, while ours yields a fairly constant value of  $C$  across the entire relative frequency shift range.

#### V. $g$ -FACTOR AND THE $f$ -WAVE PAIRING STRENGTH

We can use our results for  $A$  to determine the  $g$ -factor of the ISQ. As the theoretical predictions<sup>8,9</sup> for both the dispersion and  $g$  were made for  $\omega \sim \Omega$ , our data cannot be used directly to calculate  $g$ . We must extrapolate that

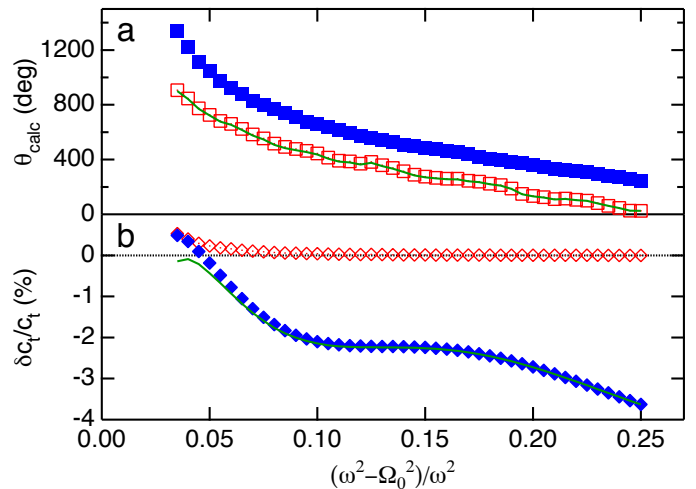


FIG. 4. A comparison of the relative importance of linear, quadratic, and cubic field dependences on, a)  $\theta_{\text{calc}}$  and b)  $\delta c_t / c_{t0} = (c_{t\text{calc}} - c_{t0}) / c_{t0}$  at  $H = 0.1$  T. Here  $\theta_{\text{calc}}$  and  $c_{t\text{calc}}$  are the rotation angle and sound velocity calculated by solving the dispersion for  $q_{\pm}$  and inserting the result into Eqs. 6 and 7;  $c_{t0}$  is calculated at zero field. These calculations use Eq. 5 with only the linear term, red open symbols; the linear and quadratic terms, green lines; and linear, quadratic, and cubic field terms, blue solid symbols. Adding the quadratic dependence is seen to change  $\theta_{\text{calc}}$  very little, and  $\delta c_t / c_{t0}$  a significant amount. Note that the quadratic field dependence, the  $B$  term, is just an upper bound from our measurement of the field dependence of  $c_t$  dictated by the precision of our measurement. Adding the cubic dependence changes  $\theta_{\text{calc}}$  significantly, and  $\delta c_t / c_{t0}$  very little, apart from very near the ISQ.

data to  $\omega = \Omega_0$  in order to compare with the theory, and doing so we obtain  $g = 0.052 \pm 0.0009$ , shown as a solid red circle in Fig. 5(a).

Previous measurements of  $g$  for the ISQ have been reported. Using the acoustic Faraday effect, Lee *et al.*<sup>3</sup> found  $g = 0.02 \pm 0.002$  at  $P = 4.32$  bar, and Davis *et al.*<sup>6</sup> measured  $g$  at pressures from  $\sim 3 - 31$  bar. An error was made in the original calculations of Davis *et al.*, later corrected,<sup>14</sup> but there was also a fundamental problem underlying the analysis which we have revised in the present work. We refer to this as reanalyzed data in Figs. 3 and 5(a). Davis *et al.* extrapolated their data to  $T = 0$  in order to avoid a region where  $g$  exhibited an unexpected temperature dependence, which disagreed with the predictions of Sauls and Serene.<sup>9</sup> Upon further investigation in the present work, we find that this temperature dependence is actually the same  $(\omega^2 - \Omega_0^2)/\omega^2$  dependence in linear magnetic field term, as shown in Fig. 2(b), that falls outside the range of validity of the theory. This can be seen in the Davis *et al.* data for 4.7 bar, which we have reanalyzed using the methods described above, shown as blue diamonds in Fig. 3(a). After reanalyzing their data for all pressures, we perform the same extrapolation as for our data to get the  $g$  values shown by solid blue diamonds in Fig. 5(a). Due to the greater



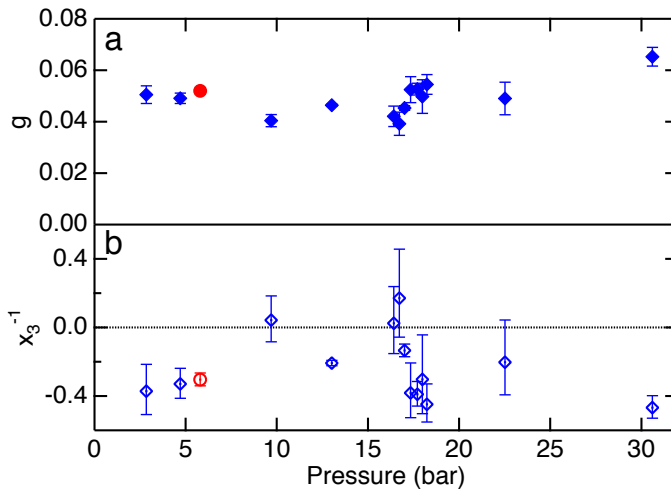


FIG. 5. (a) Extrapolated zero-shift  $g$  values for this work (solid red circle, error bars inside the data point) and re-analyzed data of Davis *et al.*<sup>6</sup> (solid blue diamonds). In the absence of Fermi liquid interaction effects, the expected weak-coupling value of  $g$  for these temperatures and pressures varies between 0.033 and 0.04, well below most of these results. (b)  $f$ -wave pairing parameter values calculated from  $g$  values in (a). Data from this work (open red circle) and Davis *et al.* (open blue diamonds) are presented. Positive values correspond to repulsive interactions, and negative values to attractive interactions; the data generally indicates attractive  $f$ -wave pairing. Error bars for Davis *et al.* data are from the extrapolation fit only, and do not include systematic effects, which are significant.

number of initial  $A$  values in the current work, and their closer proximity to the mode, our extrapolated  $g$  value is more precise than that of Davis *et al.*, with our error bars smaller than the size of the data point; the error bars for the reanalyzed data are solely from the fit, and do not reflect possible inaccuracies in our extrapolation.

The precise determination of the  $g$ -factor of the ISQ has impact beyond understanding the Zeeman splitting of the mode, since the  $g$ -factor is sensitive to  $f$ -wave pairing interactions. We use the parameter  $x_3^{-1} \equiv 1/\ln(T_3/T_c)$  to quantify the strength of these interactions, where  $T_3$  would be the transition temperature for pairing in the  $l = 3$  angular momentum channel in the absence of other interactions. Negative values of  $x_3^{-1}$  correspond to an attractive interaction.<sup>9,15</sup>

Previous experiments have measured  $x_3^{-1}$  at various pressures. The zero-field frequencies of both the ISQ and another collective mode with  $J = 2$ , the real squashing mode (RSQ), were predicted to depend on  $f$ -wave interactions,<sup>16</sup> as was the magnetic susceptibility.<sup>12,17</sup> For pressures around 6 bar,  $x_3^{-1}$  calculated from the RSQ frequency is  $-0.06$ ,<sup>15,18</sup> and two different ISQ frequency

measurements gave  $x_3^{-1}$  to be  $-0.14$ ,<sup>15,19</sup> and  $0.025$ .<sup>5</sup> In addition to uncertainty in these values from the insensitivity of the zero-field mode frequency to  $x_3^{-1}$ , there are also uncertainties in the values of the Fermi liquid parameters  $F_2^a$  and  $F_2^s$ , required for the analysis, such that a change in  $F_2^a$  or  $F_2^s$  of 0.2, within the uncertainty of the parameters, causes a change in  $x_3^{-1}$  of about 0.05. Susceptibility measurements,<sup>20</sup> at less than 1 bar, have been interpreted<sup>17</sup> to give  $x_3^{-1} = -1.75 \pm 0.15$ .

We can also calculate  $x_3^{-1}$  from  $g$ , using the theory of Sauls and Serene.<sup>9</sup> Sauls used the  $g$  measurement of Lee *et al.*<sup>3</sup> to calculate<sup>8</sup>  $x_3^{-1} \simeq -0.33$ . We calculate  $x_3^{-1}$  from both our  $g$  value and the reanalyzed data of Davis *et al.*,<sup>6</sup> shown in Fig. 5(b), where our result is an open red circle and the reanalyzed data of Davis *et al.* are open blue diamonds. While there is significant scatter, the general trend appears to agree with that of our data point,  $x_3^{-1} = -0.304 \pm 0.037$ . These results are calculated using the Fermi liquid parameter  $F_2^s$  cited by Halperin and Varoquaux<sup>15</sup> and changing  $F_2^s$  by  $\pm 0.5$  causes a change in  $x_3^{-1}$  of  $\mp 0.267$ , such that small changes in  $F_2^s$  or  $F_2^a$  could bring the current result into agreement with the RSQ measurements. Compared with the other ISQ measurements our result agrees with the previous Faraday effect data,<sup>3,6,8</sup> but not the susceptibility data,<sup>17,20</sup> other than the conclusion that the  $f$ -wave pairing interaction is attractive at low pressure.

## VI. CONCLUSION

We find significant nonlinear field effects in the dispersion relation for transverse sound in superfluid  $^3\text{He}$ . Theoretical predictions based on  $qv_F/\omega \ll 1$  for the dispersion of transverse sound are applicable in a small frequency range above the mode frequency. Theoretical results over a wide frequency range with  $qv_F/\omega \sim 1$  are needed. We have introduced a model through which we have analyzed our data and quantify the field dependence of the dispersion up to cubic order. From the linear behavior, we determined the  $g$ -factor for the Zeeman splitting of the imaginary squashing mode, which implies a small but attractive  $f$ -wave pairing interaction at low pressure. Our result for the  $f$ -wave pairing interaction parameter,  $x_3^{-1} = -0.397 \pm 0.075$  at  $P = 6$  bar, is in agreement with our interpretation of the measurements of Davis *et al.*<sup>6</sup> for which the  $l = 3$  pairing channel is attractive at all pressures.

## VII. ACKNOWLEDGMENTS

We would like to thank J.A. Sauls for his help with this work and A.M. Zimmerman for useful discussions, and acknowledge the support of the National Science Foundation, DMR-1103625.

- 
- <sup>1</sup> L. D. Landau, Sov. Phys. JETP **5**, 101 (1957).
  - <sup>2</sup> G. F. Moores and J. A. Sauls, JLTTP **91**, 13 (1993).
  - <sup>3</sup> Y. Lee, T. M. Haard, W. P. Halperin, and J. A. Sauls, Nature **400**, 431 (1999).
  - <sup>4</sup> J. P. Davis, J. Pollanen, H. Choi, J. A. Sauls, and W. P. Halperin, Nature Phys. **4**, 571 (2008).
  - <sup>5</sup> J. P. Davis, H. Choi, J. Pollanen, and W. P. Halperin, Phys. Rev. Lett. **97**, 115301 (2006).
  - <sup>6</sup> J. P. Davis, H. Choi, J. Pollanen, and W. P. Halperin, Phys. Rev. Lett. **100**, 015301 (2008).
  - <sup>7</sup> D. Rainer and J. W. Serene, Phys. Rev. B **13**, 4745 (1976).
  - <sup>8</sup> J. A. Sauls, in *Topological Defects and Non-Equilibrium Dynamics of Symmetry Breaking Phase Transitions*, Proceedings of the NATO Advanced Study Institute, held in Les Houches, France, 16-26 February 1999 No. 549, edited by Y. M. Bunkov and H. Godfrin (Kluwer Academic Publishers, eprint arXiv:cond-mat/9910260, 2000) pp. 239–265.
  - <sup>9</sup> J. A. Sauls and J. W. Serene, Phys. Rev. Lett. **49**, 1183 (1982).
  - <sup>10</sup> R. Movshovich, E. Varoquaux, N. Kim, and D. M. Lee, Phys. Rev. Lett. **61**, 1732 (1988).
  - <sup>11</sup> N. Schopohl, M. Warnke, and L. Tewordt, Phys. Rev. Lett. **50**, 1066 (1983).
  - <sup>12</sup> R. S. Fishman and J. A. Sauls, Phys. Rev. B **33**, 6068 (1986).
  - <sup>13</sup> J. A. Sauls, Y. Lee, T. M. Haard, and W. P. Halperin, Physica B **284-288**, 267 (2000).
  - <sup>14</sup> J. P. Davis, H. Choi, J. Pollanen, and W. P. Halperin, Phys. Rev. Lett. **107**, 079903 (2011).
  - <sup>15</sup> W. P. Halperin and E. Varoquaux, in *Helium Three*, Modern Problems in Condensed Matter Sciences, Vol. 26, edited by W. P. Halperin and L. P. Pitaevskii (Elsevier, 1990) Chap. 7, p. 353.
  - <sup>16</sup> J. A. Sauls and J. W. Serene, Phys. Rev. B **23**, 4798 (1981).
  - <sup>17</sup> R. S. Fishman and J. A. Sauls, Phys. Rev. B **38**, 2526 (1988).
  - <sup>18</sup> P. N. Fraenkel, R. Keolian, and J. D. Reppy, Phys. Rev. Lett. **62**, 1126 (1989).
  - <sup>19</sup> M. W. Meisel, O. Avenel, and E. Varoquaux, Jpn. J. Appl. Phys. **26-3**, 183 (1987).
  - <sup>20</sup> R. F. Hoyt, H. N. Scholz, and D. O. Edwards, Physica B+C **107**, 287 (1981).